TITLE: Formation, Mechanical and Electrical Properties of Ni-based Amorphous Alloys and their Nanocrystalline Structure

Mat. Res. Soc. Symp. Proc. Vol. 740 © 2003 Materials Research Society I10.4

Formation, Mechanical and Electrical Properties of Ni-based Amorphous alloys and their Nanocrystalline Structure

Xiangcheng Sun[1] and Tiemin Zhao[2]

[1]Center for Materials for Information Technology, The University of Alabama, Tuscaloosa, Alabama, 35487-0209
[2]Lab of RSA, Institute of Metal Research, CAS, Shenyang, P. R. China

ABSTRACT

A Ni-based amorphous alloy in $Ni_{60}Ti_{20}Zr_{20}$ system was prepared by melting spinning. The glass transition temperature (T_g) was as high as about 760 K, the supercooled liquid region was quite wide, ΔT_x = 50 K (ΔT_x= T_x-T_g, T_x crystallization temperature), and the reduced glass transition temperature (T_g/T_m) was 0.60. The amorphous alloys exhibited a high tensile strength (σ_f= 1015 MPa) at room temperature. The electrical conductivity obeyed a $T^{1/2}$ law over the range of 15 K< T < 300 K, which can be explained by an electron-electron interaction model. After annealing the amorphous alloy into primary crystallization, a nanocomposites consisted of metastable Ti_2Ni and Zr_2Ni nanophases with size less than 15 nm embedded in the amorphous matrix was appeared.

INTRODUCTION

Binary alloys can be stabilized by adding a third element which has an atomic size different from the other two elements [1], and, if that element has a very low heat of mixing with one of the other elements. Ni-Ti [2], and Ni-Zr [3] binary alloy systems have been prepared by mechanically alloying (MA) over wide composition ranges due to the large negative heat of mixing. From the related studies [4, 5], one expects that if an appropriate amount of Zr was added into Ni-Ti or Ti was added into Ni-Zr binary alloys, the glass forming ability (GFA) both Ni-Ti and Ni-Zr may be greatly enhanced. As important engineering materials, a number of Ni-based amorphous ternary alloys had ever been produced in Ni-Fe-B [6], Ni-Si-P-B [7] and Zr-Ni-M (M=Pd, Au, Pt) [8, 9] by melting spinning. It is rather important for the future progress of bulk amorphous alloys to fabricate new Ni-based amorphous alloys that high glass forming ability (GFA), good mechanical properties and high corrosion resistance. On the other hand, it is also the aim of the present work to investigate the amorphization possibility and their corresponding mechanical and physical properties. From both fundamental and technological points of view, it will be useful to optimize the microstructure, and to develop economic bulk Ni-based amorphous alloys.

EXPERIMENTAL

99.99% pure Ni, Zr, and Ti were melted and cast into ingots of nominal composition $Ni_{60}Ti_{20}Zr_{20}$ by non-consumable arc melting under a highly pure argon atmosphere. Amorphous alloy ribbons (about 3 mm wide, 0.02 mm thick) were derived by melt spinning onto a copper wheel from the $Ni_{60}Ti_{20}Zr_{20}$ ingots.

The thermal properties were measured by differential scanning calorimetry (DSC, TA Instruments model) at a heating rate of 40 K/min. The values of the glass transition temperature T_g, the onset temperature for first crystallization peak T_x, were determined from the DSC curves with an accuracy of ±1 K. Isothermal annealing of the alloys ribbon samples encapsulated in quartz tubes was carried out in vacuum of 1×10^{-5} Torr. The phase and structure of as-quenched and annealed samples were determined by x-ray diffraction with Cu K_α radiation and transmission electron microscopy (TEM, JEOL2010, operated at 200kV). The d.c. resistance was measured by the conventional four-probe method over a temperature range of 15 to 300 K. The voltages were recorded by a nanovoltmeter (model 182, Keithley Inc.) and the temperature was controlled within an accuracy of ± 0.5 K. Mechanical properties were measured at room temperature at a strain rate of 10^{-4} s^{-1} using a Gleeble 1500 testing machine. The amorphous $Ni_{60}Ti_{20}Zr_{20}$ ribbon samples with width of 3 mm and length of 5~5.5 mm were polished carefully before testing. Tensile fracture surface morphology of the samples was observed by scanning electron microscopy (SEM).

RESULTS AND DISCUSSION

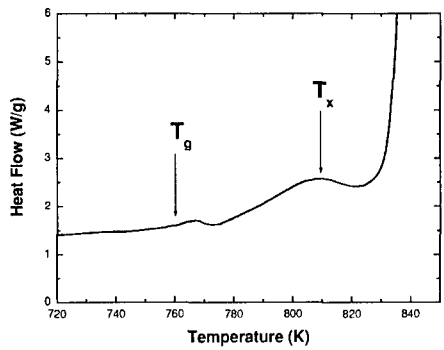

Figure 1. DSC curve of the as-quenched $Ni_{60}Ti_{20}Zr_{20}$ amorphous ribbon at the heating rate of 40K/min.

Fig. 1 shows a DSC curve of the as-quenched $Ni_{60}Ti_{20}Zr_{20}$ amorphous alloys. The glass transition is observed and its onset temperature, T_g is 760 K. The crystallization proceeds with a single exdothermic peak of which the onset temperature, T_x is 810K. It has been predicted that from kinetic considerations [6, 11], the tendency to form the amorphous phase is closely related to the reduced glass temperature (T_g/T_m, where T_m is the melting temperature) of alloys. The larger the value of T_g/T_m, the greater tendency to form the amorphous. It is evident that this Ni-based metallic amorphous alloys exhibit a wide supercooled liquid region, which reaches ΔT_x = 50K ($\Delta T_x = T_x - T_g$, where T_x is crystallization temperature), and high reduced glass transition temperature (T_g/T_m, T_m measured as 1260 K) is 0.60.

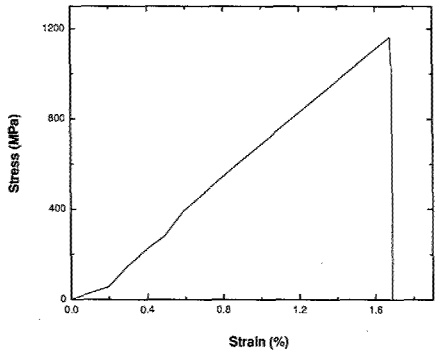

Figure 2. Stress-strain curves at room temperature for the as-quenched $Ni_{60}Ti_{20}Zr_{20}$ ribbon.

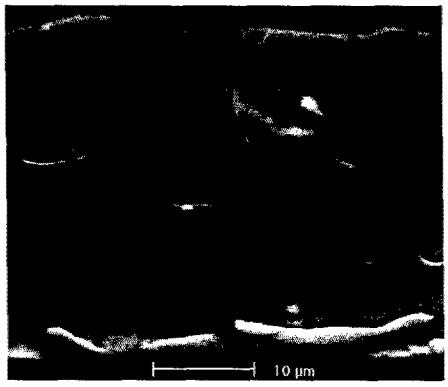

Figure 3. Scanning electron micrograph of the tensile fracture surface for the as-quenched $Ni_{60}Ti_{20}Zr_{20}$ amorphous ribbon, that clear vein patterns are visible.

Fig. 2 shows the stress-strain curve for the cylindrical samples (3 mm diameter × 5mm length) in as-quenched amorphous single-phase. It is clear that this $Ni_{60}Ti_{20}Zr_{20}$ metallic amorphous alloys exhibits high yield strength of 1015 MPa and relatively small plastic elongation of about 1.62%, where the good bending ductility is maintained in the $Ni_{60}Ti_{20}Zr_{20}$ metallic amorphous alloys. Usually, tensile fracture occurs along the maximum shear plane, which is declined by about 45° to the direction of tensile load and the fracture surface consists mainly of a vein pattern [10]. The SEM image in Fig. 3 shows that the tensile fracture surface is rather smooth on a macroscopic scale and consists mainly of well-developed vein patterns. In agreement with the model predicted by Inoue [12], the intergranular amorphous phase keeps good ductile nature and the fracture occurs preferentially along the intergranular amorphous region.

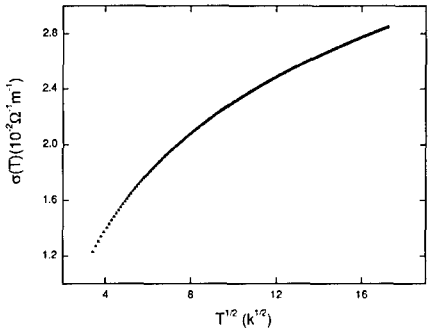

Figure 4. Electrical conductivity as a function of $T^{1/2}$ for the as-quenched $Ni_{60}Ti_{20}Zr_{20}$ amorphous ribbon.

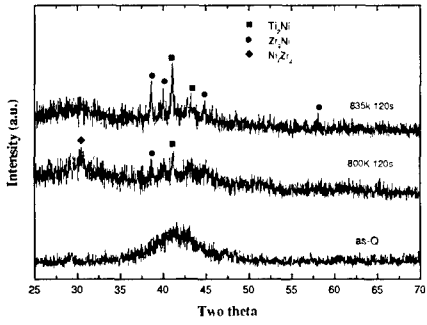

Figure 5. X-ray diffraction patterns for as-quenched and annealed $Ni_{60}Ti_{20}Zr_{20}$ alloy ribbons.

The d. c. conductivity σ (T) (Fig.4) increases with increasing temperatures range from 15 to 300K obeys a $T^{1/2}$ law; exhibiting non-metallic behavior; which can be explained by an electron-electron interaction model [13]. Such a $T^{1/2}$ law was observed for three-dimensional disordered or amorphous systems [14], in other words, this confirms the amorphous nature of the $Ni_{60}Ti_{20}Zr_{20}$ metallic alloys from 15K to 300K.

The diffraction pattern (Fig.5) of the as-quenched sample consists only of a broad peak, indicating that it is composed of an amorphous phase. For the sample annealed at 800K, the temperature just after the first crystallization peak, several very weak crystalline peaks are observed; corresponding to the tetragonal Zr_2Ni (space group I 4/mcm, a= 0.649 nm, C= 0.528 nm) and the cubic Ti_2Ni (space group, Fd3m, a= 1.1278 nm) phases. One weak peak of Ni_7Zr_2 was also found in Fig. 5(b). The broad half widths of these peaks indicate that the precipitated crystals are very fine. Zr_2Ni, Ti_2Ni and Ni_7Zr_2 phases are

metastable and these small particles should grow into larger particles upon further annealing [15]. After annealing the sample at 835K for 120s, the peaks of the Zr_2Ni and Ti_2Ni phases indeed showed higher intensity and the peak of the metastable Ni_7Zr_2 phase disappeared.

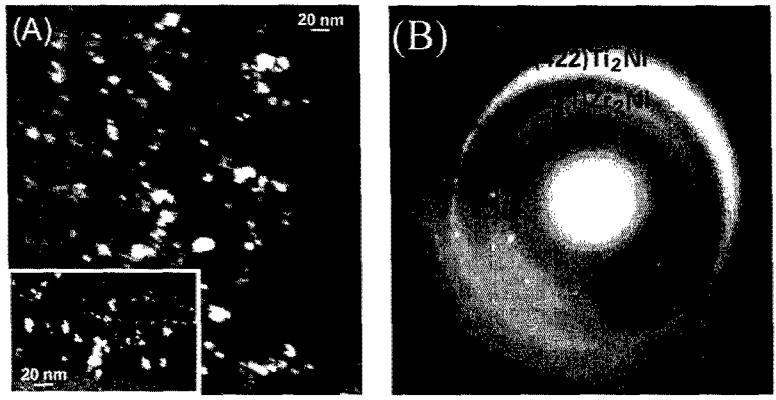

Figure 6. Dark-field TEM image (**a**) and selected area electron diffraction pattern (**b**) of the $Ni_{60}Ti_{20}Zr_{20}$ amorphous ribbon annealed at 835 K for 120 s.

The dark-field TEM image (Fig.6a) and selected-area electron diffraction pattern (Fig. 6b) of the ribbons after primary crystallization by annealing at 835K for 120s shows very fine particles with an average diameter value of 15nm surrounded by the residual amorphous phase. The particles were distributed homogeneously and had a nearly spherical morphology. The selected-area electron diffraction patterns demonstrate that these nanophases were metastable crystalline phases of Ti_2Ni and Zr_2Ni. Furthermore, together from the above XRD patterns for the samples with different temperature treatments, only a little fraction of Ti_2Ni and Zr_2Ni phases had been observed after annealed at 800k at 120s. This indicated, within the exdothermic peak, there was more metastable crystalline phase precipitated (i.e. Ni_7Zr_2 phase appeared) from the amorphous matrix. This suggested that the reaction in the DSC curve corresponded to the formation of the primary Ti_2Ni and Zr_2Ni phases [16].

CONCLUSIONS

A new Ni-based amorphous alloy ($Ni_{60}Ti_{20}Zr_{20}$) having a wide supercooled liquid region was successfully prepared. The amorphous alloy exhibited good ductility with a tensile strength (σ_f) as high as 1015 MPa at room temperature. Electrical conductivity measurement confirmed the amorphous nature of this alloy. After primary crystallization, a nanocomposite composed of two metastable Ti_2Ni and $NiZr_2$ nanophases embedded in the amorphous matrix was formed. The formation of this kind of Ni-based amorphous alloy, together with a large supercooled liquid region and high glass-forming ability, offer us

good opportunities for the future development of bulk Ni-based amorphous alloys as basic science and engineering materials.

REFERENCES

1. R. B. Schwarz and C. C. Koch, *Appl. Phys. Lett.* **49**, 146 (1986).
2. K. Y. Wang, T. D. Shen, H. G. Jiang, M. X. Quan and W. D. Wei, *Mater. Sci. Eng.* **A179/A180**, 215 (1994).
3. P. Y. Lee and C. C. Koch, *J. Mater. Sci.* **23**, 2837 (1988).
4. K. Amiya, N. Nishiyama, A. Inoue and T. Masumoto, *Mater. Sci. Eng.* **A179/A180**, 692 (1994).
5. V. V. Molokanov, V. N. Chebotnikov, *J. Non-Crystalline Solids* **117/118**,789 (1990).
6. Y. Waseda, S. Ueno, M. Hagiwara and K.T. Aust, Prog. Mater. Sci. **34**, 149 (1990).
7. F. E. Luborsky, *Mater. Sci. Eng.* **28**, 139 (1977).
8. J. Saida, M. Matsushita, C. Li and A. Inoue, *Appl. Phys. Lett.* **76**, 3558 (2000).
9. B. S. Murty, D. H. Ping, K. Hono and A. Inoue, *Appl. Phys. Lett.* **76**, 55 (2000).
10. M. W. Chen, T. Zhang, A. Inoue, A. Sakai and T. Sakurai, *Appl. Phys. Lett.* **75**,1382 (1999).
11. D. Turnbull, *Contempt. Phys.* **10**, 473 (1969).
12. A. Inoue, *Acta Mater.* **58**, 279 (2000).
13. K. Lal, A. K. Meikap, S. K. Chattopadhyay, S. K. Chatterjee, M. Ghosh, A. Barman and S. Chatterjee, *Solid State Commun.* **113**, 533 (2000).
14. A. K. Meikap, A. Das, S. Chatterjee, M. Digar and S. N. Bhattacharyya, *Phys. Rev.* **B47**, 1340 (1993).
15. C. Fan, C. F. Li and A. Inoue, *J. Non-Crystalline Solids* **270**, 28 (2000).
16. J. G. Wang, B. W. Wang, B. W. Choi, T. G. Niegh and C. T. Liu, *J. Mater. Res.* **15**, 798 (2000).